Quantum Electronics **33** (9) 798 – 802 (2003)

ACTIVE MEDIA. LASERS

PACS numbers: 42.55.Lt; 42.60.Da; 42.60.Jf
DOI: 10.1070/QE2003v033n09ABEH002501

Single-frequency oscillation of a wide-aperture krypton laser

S.A. Babin, S.V. Khorev

Abstract. **The parameters of a high-current krypton discharge in tubes of an increased diameter (5 – 7 mm) are studied and optimised. Increased lasing power on the lines of singly and doubly charged krypton ions is achieved: 14 W (647 – 676 nm) and 6 W (407 – 415 nm). One transverse and one longitudinal mode are selected with efficiencies of 85 and 70 % using a convex – concave resonator and a Fabry – Perot etalon, respectively. The shape of the Lamb dip at the 676-nm line is studied in the single-frequency oscillation mode. It is shown that, in accordance with the theory, the dip broadens by a factor of 2.6 due to Coulomb ion – ion collisions at an achieved electron concentrationв $N_e \sim 5 \times 10^{14}$ cm^{-3}.**

Keywords: *wide-aperture laser, krypton ion laser, mode selection, single-frequency lasing, Lamb dip, Coulomb broadening.*

1. Introduction

Higher requirements to the quality of laser radiation are determined by the development of research methods and laser technologies. Various mode-selection methods are used to narrow the lasing spectrum and obtain Gaussian beams [1, 2]. High-power ion lasers are characterised by the presence of many transverse modes, since the power per unit discharge length is proportional to the discharge-channel diameter [3]. In this case, the transverse-mode selection using a diaphragm in a conventional stable resonator is inefficient because the transverse size of the axial TEM_{00} mode is $w \sim 1$ mm (for a resonator length $L \sim 1$ m), which is much smaller than the discharge-channel diameter $d \geqslant 5$ mm for wide-aperture ion lasers. In addition, due to a significant Doppler broadening of the laser line (5 – 10 GHz), many competing longitudinal modes usually participate in lasing [4].

High-power lasing and mode selection in wide-aperture ion lasers were achieved and studied using the most widespread argon laser. The main transverse lasing mode was selected using the so-called multimirror telescopic resonators, whose selection efficiency in a laser with $d = 7$ mm was no higher than ~ 40 % [5], and a two-mirror convex – concave resonator that allowed the efficiency to be increased to ~ 70 % [6]. The longitudinal modes were selected using mainly a tilted intracavity Fabry – Perot etalon. The selection efficiency of the etalon in telescopic resonators was ~ 40 % [5], and the single-frequency lasing power was at most $0.4 \times 0.4 \simeq 1/6$ of the multimode lasing efficiency, which is comparable with the power of single-frequency capillary lasers despite large advantages of wide-aperture lasers in a multimode regime. This problem was also solved using a convex – concave resonator, in which the Fabry – Perot etalon can select in a nontilted position and introduces lower losses. Thus, the total efficiency of single-frequency lasing was increased to $0.7 \times 0.7 \simeq 1/2$ [7].

Single-frequency lasers are the basic tool of nonlinear Doppler-free spectroscopy. The Lamb dip [8] observed in the frequency dependence of the laser power is an example of the simplest nonlinear spectral resonance. A significantly broadened Lamb dip was observed in argon lasers. It has been recently revealed that this broadening is caused by Coulomb ion – ion scattering [9]. Note that more intricate nonlinear effects [10] were studied only in an argon laser. Data for other noble gases, such as krypton, are almost absent.

This work is aimed at the mode selection and obtainment of single-frequency lasing in a wide-aperture krypton laser, as well as the study of the Lamb dip and its broadening due to ion – ion collisions. Solving this problem required measurements of the plasma parameters of a high-current krypton discharge in tubes of an increased diameter ($d = 5 - 7$ mm). As a result of optimising the discharge and resonator parameters, efficient lasing on the lines of singly and doubly charged krypton ions has been achieved.

2. High-current discharge and multimode lasing in krypton

The decisive effects occurring at high currents in ion lasers are the gas-transfer processes [4]: on the one hand, the gas is displaced from the discharge-column zone into the cold regions and, on the other hand, moves along the discharge column due to electrophoresis. The appearance of an electrophoresis force is caused by the fact that electrons transfer their momentum to neutral atoms in collisions, while the momentum of ions is transferred to the tube walls [11]. As a result, a force F, directed from the cathode to the anode, induces a pressure gradient along the discharge and acts on the gas. A conventional connection of the anode

S.A. Babin, S.V. Khorev Institute of Automation and Electrometry, Siberian Branch, Russian Academy of Sciences, prosp. Akad. Koptyuga 1, 630090 Novosibirsk, Russia; e-mail: babin@iae.nsk.su

Received 9 December 2002
Kvantovaya Elektronika **33** (9) 798 – 802 (2003)
Translated by A.S. Seferov

and cathode with a bypass canal does not completely eliminate this gradient, since the latter is needed for gas circulation. A scheme with a forced gas circulation offers additional opportunities [12]. The gas circulation direction must obviously coincide with the electrophoresis direction, and the longitudinal equalising could be achieved by balancing the gas admission and evacuation rates [13, 14].

An 'equilibrium' atomic concentration $N_0 = (Q + I_i)/(BF)$ is a parameter of a longitudinal-flow discharge. The gas-flow rate Q is an external parameter, and the ion flow I_i, the channel resistance B^{-1}, and the electrophoresis force F increase with the discharge current I_i at a given flow rate Q. The resulting change in $N_0(I)$ is of interest. Argon pressure measurements through a small hole in the discharge channel $p(I) \sim N_0(I)$ have shown [14] that the equilibrium concentration is virtually current-independent, being approximately proportional to the flow rate Q. The results of similar measurements in a tube with $d = 7$ mm for krypton under the same conditions, which corresponded to the minimum laser output, are shown in Fig. 1a. The pressure p in the discharge also changes weakly over a wide current range. However, at limiting values $I \gtrsim 150$ A, which are close to the appearance of instabilities, the pressure appreciably falls. The electron concentration N_e measured by the nonlinear dispersive interferometry technique [15] increases linearly with the current almost in the entire range, and a saturation caused by a pressure decrease is observed at high currents. Thus, a longitudinal-flow discharge in krypton is similar to a discharge in argon; differences in these dependences are observed only at high currents. This effect is primarily determined by a higher degree of ionisation achieved in krypton due to its lower ionisation potential. When the optimal concentration of neutral atoms during lasing is lower ($N_a \sim 10^{14}$ cm^{-3}), the electron concentration N_e in krypton is approximately twice as high as in argon with the same tube [14]. The degree of ionisation in krypton is estimated at $N_e/N_a = 0.3-0.4$. This must lead to a significantly broadened Lamb dip considered below.

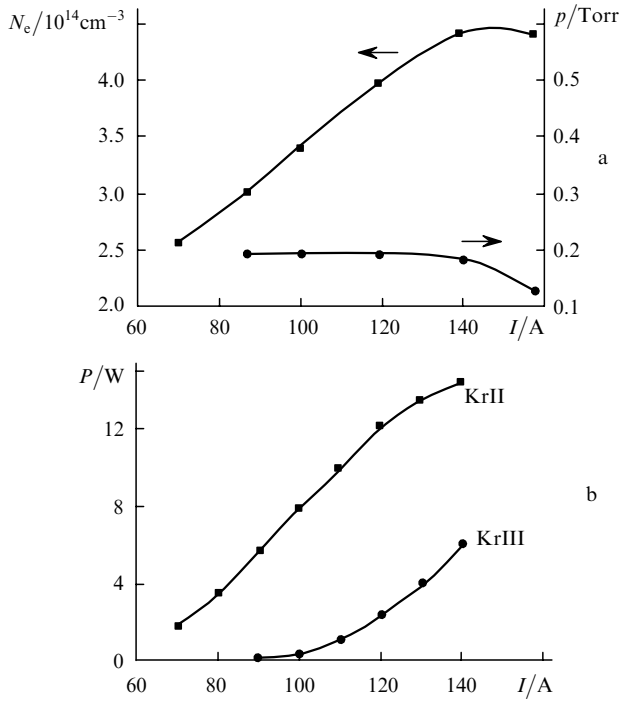

Figure 1. (a) Electron concentration N_e, pressure p, and (b) output power P at the KrII and KrIII lines as functions of the current I.

Due to a high degree of ionisation, we can also expect an earlier output-power saturation on the lines of KrII singly charged ions (compared to ArII lines) depending on the discharge current, which was confirmed experimentally (Fig. 1b). As is known, the main cause of the output-power saturation in argon is a double ionisation [4], which manifests itself in krypton at lower currents. On the one hand, this limits the power on the KRII lines, the most intense of which are 647- and 676-nm lines. On the other hand, the lasing power on KrIII violet lines (407, 413, and 415 nm) is comparable to the power on red lines already at comparatively low currents $I \sim 140$ A. Thus, lasing on the short-wavelength lines of doubly ionised krypton has a lower threshold and higher relative power than in an argon laser.

3. Selection of the fundamental transverse mode

Effective suppression of higher transverse modes is usually achieved by their loss discrimination with an increase in the number of Fresnel zones in the resonator ($N = d^2/4\lambda L$, L is the resonator length, d is the aperture diameter, and λ is the wavelength). However, in standard resonator configurations, this requires either a decrease in d or increase in L, which is usually unacceptable. More complex resonators, such as telescopic ones (TRs) contain a large number of optical surfaces and introduce considerable losses for the fundamental mode. Like in an argon laser, to select the TEM_{00} mode in the wide-aperture krypton laser, we used a two-mirror convex–concave resonator (CCR) in a stable regime [6]. Since the advantages of a CCR in the argon laser were more significant for weak lines, this choice is of essential importance for the krypton laser with a low gain ($g = 0.05 - 0.15$ m^{-1}) for almost all lasing lines.

A qualitative picture of an increase in the mode volume in the CCR is that the mirrors form the diverging part of the Gaussian beam, which is far from the waist (Fig. 2); at $L > |R_2| - |R_1|$ the resonator is stable (R_1 and R_2 are the radii of the convex and concave mirrors, respectively). In analogy with the TR, we introduce the effective length of the CCR as $L_{eff} \sim R_2 \simeq -R_1$; the effective Fresnel number is then defined as $N_{eff} = d^2/4\lambda L_{eff}$. An efficient selection with a good medium filling factor is possible at $L_{eff} \gg L$, when the condition $w \simeq (\lambda L_{eff})^{1/2} \sim (\lambda R_2)^{1/2} \sim d$ is valid [w is the caustic diameter of the resonator mirrors, and d is the diameter of the active medium (Fig. 2a)]. The necessary discrimination of higher modes was obtained in argon lasers with a discharge-channel diameter $d = 5 - 7$ mm at $R_2 \simeq -R_1 \sim 10$ m and a comparatively low (~ 0.5 %) diffraction loss of the fundamental mode [6].

TEM_{00}-mode lasing with a power $P_0 \simeq 3$ W was obtained on the strong 647-nm KrII line in a CCR with parameters $R_1 \simeq -14$ m, $R_2 \simeq 10$ m, and $L = 1.1$ m in a discharge tube with $d = 5$ mm, a length $l = 55$ cm, and a Brewster window at a current $I = 100$ A. This power was virtually equal to the multimode power in a semisymmetric (plane–concave) resonator ($P = 3.5$ W). The selection efficiency was $P_0/P \simeq 0.85$, which exceeds the corresponding parameter of an argon laser with analogous parameters and approximately corresponds to the geometrical filling of the tube. Single-mode lasing with a power of ~ 10 W at red

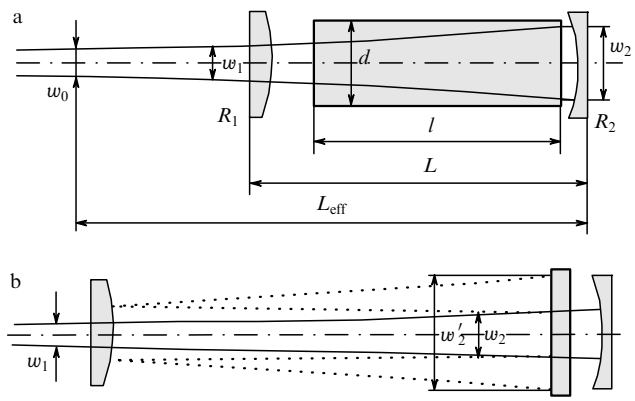

Figure 2. Basic parameters of a convex–concave resonator (a) without and (b) with an etalon.

lines (7 W at the 647-nm line) can be expected in a tube with a larger volume (as in Fig. 1b). Close values of the selection efficiency were obtained at other KrII lines. Due to the lower gain and smaller effective size of the active medium (the cross profile of doubly charged ions is appreciably narrower), the weaker KrIII violet lines allowed the axial mode to be also selected quite efficiently in a semisymmetric plane–concave resonator with a diaphragm. In this case, the use of a CCR was inexpedient. Note that the selection-efficiency values for tubes with Brewster windows and vacuum mirrors in a krypton laser were close to each other, in contrast to an argon laser with a higher output.

4. Single-frequency generation of a cw krypton laser

An experimental setup used to study single-frequency lasing in krypton is shown in Fig. 3. It includes a krypton laser with a sectioned discharge tube (*2*) and a cold cathode [3] complemented with a Fabry–Perot etalon (*4*) in a thermostat with a thermal stabiliser (*9*). The lasing power was measured by a power meter (*1*). Axial modes were monitored by a scanning interferometer (*5*) and an oscilloscope. Transverse modes were monitored by recording both the beam's cross profile using a movable diaphragm with a detector (*6*) and the profile of intermode beats [6] using a lens (*7*) and a spectrum analyser (*8*).

The principle of the etalon operation is based on the selective transmission of the only TEM_{00} longitudinal resonator mode and removal of the other (reflected) modes from the resonator upon tilting the etalon [16]. A substantial drawback of the tilted etalon is the comparatively high loss per radiation pass, which is associated with a shift of interfering beams multiply reflected by the etalon's faces. The loss per pass is minimised near the normal etalon position relative to the axis (in the so-called zero order), but, in this case, no mode selection is observed, since parasitic radiation returns into the resonator. Nevertheless, a mode selection with an nontilted etalon is possible if one mirror of the resonator is convex [7]: the etalon-reflected light then enters the unstable resonator formed by the convex mirror and etalon, and the required loss is provided by a beam divergence during round trips, $w_2' > w_2$ (Fig. 2b). Note that a similar possibility for selecting modes also exists in the flat mirror–convex etalon configuration [17]. However, the production of an etalon with concentric surfaces involves technological difficulties, and, in this case, its parameters are strictly linked to a particular resonator configuration.

The loss per pass in the etalon in the selection scheme proposed is caused by the fact that the wave front of the beam, which is incident on the etalon, is spherical and its radius of curvature is close to that of the concave mirror (R_2). In this scheme, the interfering beams also overlap incompletely, as for the tilted etalon. The loss per pass due to this effect is estimated at $l_0 = 4rd_e/nR_2 \sim 0.07\,\%$, which is $R_2/L \sim 10$ times lower than in the tilted etalon [16]: $l_1 \simeq 4rd_e\Theta nw > 4rd_e nL \simeq 0.7\,\%$ (d_e is the etalon thickness, r is the reflectivity per surface, Θ is the tilt angle, and n is the

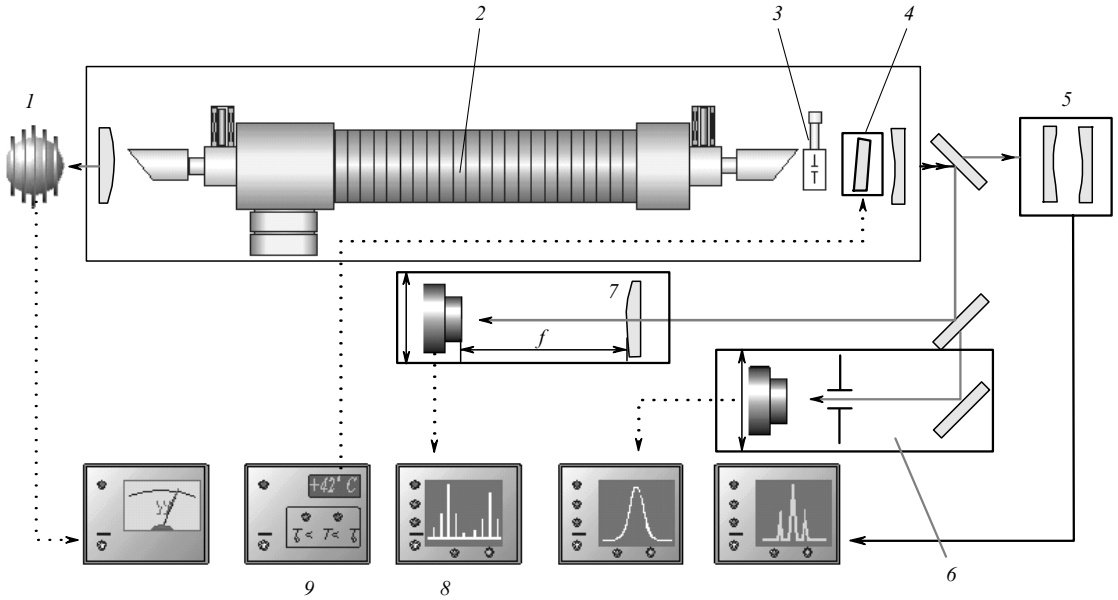

Figure 3. Schematic of the experimental setup for studying single-frequency lasing: (*1*) power meter; (*2*) discharge tube; (*3*) diaphragm; (*4*) Fabry–Perot etalon; (*5*) scanning interferometer; (*6*) detector; (*7*) lens; (*8*) spectrum analyser; and (*9*) thermal stabiliser.

refractive index of the etalon material). Typical values $L = 1$ m, $d_e = 1$ cm, $n = 1.46$, $r = 0.2$, and $R_2 = 10$ m were used in the numerical estimates. The etalon tilt angle necessary for the selection is taken equal to the beam's angular size $\Theta \sim w/L$. For an inhomogeneous line saturation, the effect of etalon losses on the output power can be separated in the form of a factor $(1 + 2l_1/t)^2$. For a mirror transmission $t = 2\,\% - 3\,\%$ corresponding to the optimal krypton-laser output power in a multimode regime (without an etalon), the single-frequency lasing powers with tilted and nontilted etalons may differ by a factor of ~ 2.

A single-frequency lasing power $P_{00} \simeq 2$ W was obtained on the strong 647-nm KrII line in a discharge tube with $d = 5$ mm and a current $I = 100$ A at an initial (single-mode) power $P_0 \simeq 3$ W. Thus, the etalon selection efficiency was $P_{00}/P_0 \simeq 0.7$. In contrast to the argon laser, a coating-free etalon introducing lower losses, which is essentially important for weak lines, was sufficient for selecting modes in the krypton laser. An almost the same selection efficiency was also obtained at other KrII and KrIII lines. The laser frequency can be tuned by a nontilted etalon only by changing its temperature. This technique was used to record the frequency dependence of P_{00} and study the Lamb dip.

5. Coulomb broadening of the Lamb dip in a single-frequency krypton laser

Measurements were carried out on the 676.4-nm line (the $5p^4P^o_{1/2}5s^2P_{1/2}$ transition) of singly charged krypton ions (KrII) with a discharge tube with $d = 5$ mm and $l = 55$ cm. The resonator consisted of a high-reflectivity (vacuum) mirror with a radius of curvature $R_2 = 10$ m and a flat mirror with a transmission $t = 2$ %. The flat mirror was used to reduce the transverse size of the mode, thus allowing the transverse discharge inhomogeneity to be neglected. The measurements were performed at the current $I = 100$ A, and the intracavity radiation intensity at the 676.4-nm line was ~ 10 W cm^{-2}. The frequency was tuned by heating the etalon. An example of the measured curve is shown in Fig. 4. Measurement errors are mainly caused by mode jumps during scanning. The asymmetry of the profile observed is related to nonlinear aperture (lens) effects [18].

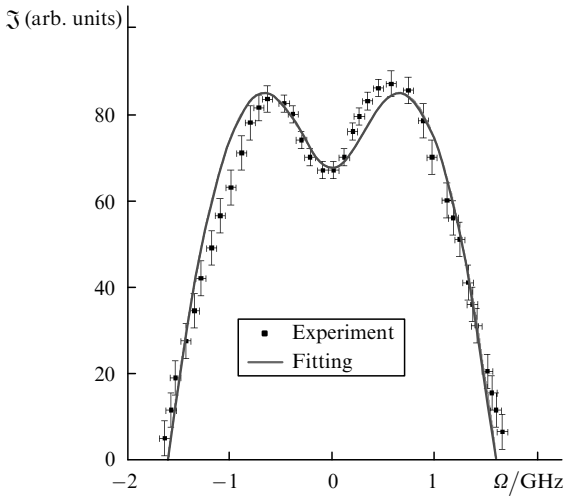

Figure 4. Output power $\Im$ as a function of the frequency detuning Ω from the line center.

We compare the experimental curve to the theory in the approximation of the Lorentzian collisional profile of the Lamb dip [9]. Coulomb ion–ion scattering leads to a change in the active-ion velocity and has a character of a diffusion in the velocity space. A diffusion-cause change in the velocity Δv_d leads to a Bennett-dip broadening in the velocity distribution of the population by a value $\Gamma_d = k\Delta v_d$ (k is the wave number). Introducing a dimensionless parameter of broadening $\gamma = (\Gamma_{mn} + \Gamma_d)/\Gamma_{mn}$, we have the Lamb-dip width [9] $\mathfrak{G} \equiv \Gamma_{mn}(\gamma + 1)/2$, where Γ_{mn} is the natural transition width and m, n are the level numbers. If the saturation is not high, the Lamb-dip profile is expressed by the formula

$$\varkappa(\Omega) = A\left[1 - \exp\frac{\Omega^2 - \Omega_t^2}{(kv_T)^2}\right]\left[1 + \frac{\mathfrak{G}^2}{\mathfrak{G}^2 + \Omega^2}\right]^{-1}, \qquad (1)$$

where $\varkappa = \Im/\Im_0$ is the dimensionless saturation parameter; $\Im$ and $\Im_0$ are the lasing and saturation intensities, respectively; Ω is the detuning relative to the profile centre; Ω_t is the lasing-quenching frequency; and kv_T is the Doppler width. Note that this approximation is valid at $\varkappa \ll \gamma$ (in our case, $\varkappa \simeq 0.8$). The radiative lifetimes of the 676.4-nm-line levels are $1/\Gamma_n \simeq 7 \times 10^{-9}$ s and $1/\Gamma_m \simeq 4.4 \times 10^{-10}$ s [4]. The kv_T value was 2.3 GHz. The data obtained were used to fit expression (1) by the weighted-least-squares method with free parameters $\mathfrak{G}$ and A, and the quenching frequency $\Omega_t = 1.6$ GHz was determined experimentally. The Lamb-dip width $\mathfrak{G}$ (FWHM) resulting from the fitting was 0.5 ± 0.03 GHz. By expressing the broadening parameter γ through the obtained dip-width value, we have

$$\gamma = 2\frac{\mathfrak{G}}{\Gamma_{mn}} - 1 = 4.2(\pm 25\,\%). \qquad (2)$$

Recall that the quantity γ characterises the Bennett-dip broadening in the velocity space, and the Lamb dip broadens by a factor of $(\gamma + 1)/2 = 2.6$. To estimate the theoretical value of γ [9], we assume that we deal with a single-component plasma:

$$\gamma = 1 + \frac{kv_T}{\Gamma_{mn}}\left(\frac{\nu_{ii}}{4\Gamma_m}\right)^{1/2}, \qquad (3)$$

where

$$\nu_{ii} = \frac{16\sqrt{\pi}\Lambda N_i e^4}{3M^2 v_T^3};$$

ν_{ii} is the frequency of ion–ion collisions; $\Lambda \simeq \lg(T_i^{3/2} \times N_e^{-1/2} e^{-3})$ is the Coulomb logarithm, T_i is the ion temperature; N_i is the concentration of ions, and M is the atomic mass. Substituting the values corresponding to the experimental conditions into (3), we obtain $\gamma \simeq 3.5$, which agrees with the experiment within the measurement error.

6. Conclusions

The methods for radiation selection in wide-aperture lasers, which had been demonstrated earlier for an example of an argon laser [6, 7], were successfully used in this study to obtain single-frequency lasing in a krypton laser, including

the selection of transverse modes in a convex–concave resonator and selection of longitudinal modes using a Fabry–Perot etalon installed normally to the resonator axis. The efficiency obtained is close to the theoretical limit.

The designed single-frequency laser was used to record the Lamb dip on krypton ions. The dip width and broadening parameter are measured. It is shown that Coulomb collisions broaden the Lamb dip by a factor of 2.6 that agrees with the theory. In addition to measurements on argon lines [9] in which the dependences of the Lamb-dip width on the ion concentration and charge had been verified, in this work, the dependence on the ion mass was verified.

Holography is an important technological application of single-frequency ion lasers. Red lines (647 and 676 nm) of the krypton laser supplement blue–green lines of the argon laser and represent the basis of colour holography. In particular, the results on single-frequency lasing obtained in this study were used in the system for recording on a polymer film, which was designed at the Research Institute of Organic Chemistry (Siberian Branch, Russian Academy of Sciences) [19] with Inversiya wide-aperture argon and krypton lasers. The opportunity of using the intense 413-nm krypton violet line is of essential importance for developing the recording technologies on a photoresist with the maximum sensitivity in this spectral region. When changing from the 457-nm argon line to the 413-nm krypton violet line, the recording-process duration decreases by a factor of ~ 10. Obtaining the second harmonic (207 nm) at this line, which may be advantageous in the technology of recording Bragg gratings [20] compared to the conventional second harmonic (244 nm) of the argon laser, seems to be promising.

Hence, the results on single-frequency lasing of a krypton laser obtained in this work have been already applied in research (nonlinear plasma spectroscopy) and laser technologies (polymer and colour holography) and can be the basis of new studies and applications.

Acknowledgements. The authors thank S.I. Kablukov, A.E. Kuklin, and M.A. Kondratenko for their help in experiments. This work was supported by Grant No. NSh-439.2003.2 of the Program of State Support of Leading Scientific Schools and a grant of the Siberian Branch of the RAS.

References

1. Smith P.W. *Proc. IEEE,* **60**, 422 (1972).
2. Anan'ev Yu.A. *Opticheskie rezonatory i lazernye puchki* (Optical Resonators and Laser Beams) (Moscow: Nauka, 1990).
3. Donin V.I. *Moshchnye ionnye gazovye lazery* (High-Power Ion Gas Lasers) (Novosibirsk: Nauka, 1991).
4. Davis C.C., King J.A., in *Advances in Quantum Electronics* (New York: Acad. Press, 1975) Vol. 3, p. 169.
5. Apolonskii A.A., Donin V.I., Timofeev T.T. *Kvantovaya Elektron.*, **13**, 1004 (1986) [*Sov. J. Quantum electron.*, **16**, 654 (1986)].
6. Babin S.A., Gershinskii G.A., Eremenko T.Yu., Timofeev T.T., Khorev S.V. *Kvantovaya Elektron.*, **21**, 121 (1994) [*Quantum Electron.*, **24**, 112 (1994)].
7. Babin S.A., Khorev S.V. *Kvantovaya Elektron.*, **27**, 42 (1999) [*Quantum Electron.*, **29**, 324 (1999)].
8. Lamb W.E. Jr. *Phys. Rev. A.*, **134**, 1429 (1964).
9. Babin S.A., Shapiro D.A. *Phys. Rep.,* **241**, 119 (1994).
10. Lebedeva V.V., Odintsov A.I., Glavatskikh N.A., Grin' L.E., Shul'ga A.G. *Zh. Prikl. Spektrosk.*, **41**, 385 (1984).
11. Chester A.N. *Phys. Rev.*, **169**, 169 (1968).
12. See B.A., Garwoli W., Hughes J.L. *IEEE J. Quantum Electron.*, **3**, 169 (1967).
13. Babin A.S., Kuklin A.E., Yatsenko A.S. Inventor's Certificate of the USSR, No. 1672901, 1991 (priority of 24.02.89).
14. Babin S.A., Kuklin A.E. *Proc. SPIE Int. Soc. Opt. Eng.*, **1397**, 589 (1991).
15. Alferov G.N., Babin S.A., Drachev V.P. *Opt. Spektrosk.*, **63**, 594 (1987).
16. Hercher M. *Appl. Opt.,* **8**, 1103 (1969).
17. Hariharan P. *Opt. Lett.*, **7**, 274 (1982).
18. Troitskii Yu.V. *Opt. Spektrosk.*, **31**, 158 (1971).
19. Sazonov Yu.A., Shelkovnikov V.V., Pen E.F., Gerasimova T.N. *Proc. SPIE Int. Soc. Opt. Eng.*, **4149**, 100 (2000).
20. Kachiyap R. *Fiber Bragg Gratings* (San Diego, London, Boston, New York, Sidney, Tokio, Toronto: Acad. Press, 1999).